ELSEVIER

Contents lists available at ScienceDirect

# Journal of Solid State Chemistry

journal homepage: www.elsevier.com/locate/jssc





# Cation exchange route to a Eu(II)-containing tantalum oxide

Shaun O'Donnell<sup>a</sup>, Eric Gabilondo<sup>a</sup>, Subhendu Jana<sup>a</sup>, Aylin Koldemir<sup>b</sup>, Theresa Block<sup>b</sup>, Myung-Hwan Whangbo<sup>a</sup>, Reinhard Kremer<sup>c</sup>, Rainer Pöttgen<sup>b</sup>, Paul A. Maggard<sup>a,\*</sup>

- <sup>a</sup> Department of Chemistry, North Carolina State University, Raleigh, NC, 27695-8204, USA
- <sup>b</sup> Institut für Anorganische und Analytische Chemie, Universität Münster, Corrensstrasse 30, 48149, Münster, Germany
- <sup>c</sup> Max Planck Institute for Solid State Research, Stuttgart, 70569, Germany

#### ABSTRACT

Traditional synthetic efforts to prepare Eu(II)-containing oxides have principally involved the use of high temperature reactions starting from EuO or a controlled, highly-reducing, atmosphere. Conversely, *chimie douce* approaches that are more amenable to the targeted syntheses of new, and potentially metastable, Eu(II)-oxides have yet to be explored. Herein, a cation-exchange route to new Eu(II)-containing oxides, e.g., EuTa<sub>4-x</sub>O<sub>11</sub> (x=0.04), has been discovered and its structure determined by powder X-ray diffraction (Space group  $P6_322$  (#182), a=6.2539(2) Å; c=12.3417(2) Å). The compound derives from the cation exchange of Na<sub>2</sub>Ta<sub>4</sub>O<sub>11</sub>, via a reaction with EuBr<sub>2</sub> at 1173 K, and replacement by half the number of divalent Eu cations. Rietveld refinements show preferential ordering of the Eu cations over one of the two possible cation sites, i.e., Wyckoff site 2d (~94%; Eu1) versus 2b (~6%; Eu2). Total energy calculations confirm an energetic preference of the Eu cation in the 2d site. Tantalum vacancies of ~1% occur within the layer of Eu cations and TaO<sub>6</sub> octahedra, and ~20% partial oxidation of Eu(II) to Eu(III) cations from charge balance considerations. <sup>151</sup>Eu Mössbauer spectroscopy measured at 78 K found a Eu(II):Eu(III) ratio of 69:31, with a relatively broad line width of the former signal of  $\Gamma=7.6(2)$  mm s<sup>-1</sup>. Also, the temperature-dependent magnetic susceptibility could be fitted to a Curie Weiss expression, giving a  $\mu_{eff}=6.2~\mu_{\rm B}$  and  $\theta_{\rm CW}=-10~{\rm K}$  and confirming a mixture of Eu(II)/Eu(III) cations. The optical bandgap of EuTa<sub>4-x</sub>O<sub>11</sub> was found to be ~1.5 eV (indirect), significantly redshifted as compared to ~4.1 eV for Na<sub>2</sub>Ta<sub>4</sub>O<sub>11</sub>. Spin-polarized electronic structure calculations show that this redshift stems from the addition of Eu  $4f^7$  states as a higher-energy valence band. Thus, these results demonstrate a new cation-exchange approach that represents a useful synthetic pathway to new Eu(II)-containing oxides for tunable magnetic and optical prope

### 1. Introduction

Rare Earth (RE) oxides are known to have many intriguing properties and which have made them one of the most interesting classes of compounds [1,2]. Currently, while most oxides that have been investigated contain the RE as a trivalent cation, less frequently can the analogous oxides be prepared where it exists as a divalent cation, e.g., containing Yb(II) or Eu(II). Within this area, research into Eu(II)-containing oxides has been long-standing, and principally stemming from their interesting magnetic and magneto-optic properties such as reported by Shafer, Greedan and many other contemporaries [3-5]. Amongst the earliest studied examples, the binary compound EuO exhibits a ferromagnetic transition at a temperature of ~77 K [6], while EuSiO<sub>4</sub> was also first reported to be optically transparent and show ferromagnetism below ~7 K [7]. Motivated by their intriguing properties and crystalline structures, several Eu(II)-based oxides were discovered in combination with early transition metal cations such as Ti(IV), Zr(IV), Nb(V) and Ta(V). Notable examples within these systems have included EuTiO<sub>3</sub>, which exhibits the magneto-restriction effect caused by a strong spin-lattice coupling [8,9], antiferromagnetic ordering in the double perovskites  ${\rm Eu}_2 Ln{\rm TaO}_6$  (Ln= trivalent rare earth) [10], as well as less understood, complex, magnetic transitions at low temperatures in  ${\rm Eu}_2{\rm Ta}_2{\rm O}_7$  [11]. Despite their tantalizing physical properties, targeted research efforts into Eu(II) oxides spanning over ~50 years have only resulted in a limited number owing to well established synthesis problems.

General guidelines have been postulated to aid in the predicted synthesizability of new Eu(II)-based oxides [12], including that a) the Sr (II) analogue should exist (owing to its similar ionic radius), b) that the other cations in the oxide must not be too easily reduced by Eu(II), and c) the compound should not fall near the boundary of that structure's stability field. While these guidelines can be useful for more conventional synthetic approaches, they may also serve to unnecessarily restrict investigations by alternative synthetic routes. The absence of more tunable synthetic routes to prepare divalent *RE* compounds is a bottleneck to many potentially interesting Eu(II) containing oxides. One alternative synthetic method amenable to targeted synthetic efforts is the use of cation exchange techniques [13,14], but which have yet to be applied to divalent *RE* oxides. Recent research activity has demonstrated

E-mail address: paul\_maggard@ncsu.edu (P.A. Maggard).

<sup>\*</sup> Corresponding author.

the broad applicability of flux-mediated ion-exchange reactions in addressing synthetic bottlenecks to technologically relevant solid-state compounds, as has been recently reviewed [15,16]. This type of reaction is enabled by using a metal salt of relatively low-melting point, whereby a metal cation of the salt (B') exchanges with a metal cation (A) of the reactant metal oxide (e.g., AMO3 + B'X2  $\rightarrow$  B'MO3 + AX2). The thermodynamic driving force for these types of reactions is typically the exothermic formation of the exchanged salt product, i.e., AX2 in the reaction, also described as thermokinetic coupling [17]. Often, these exchanges are topotactic, and thus the underlying structure of the reactant oxide can frequently be maintained in the exchanged product. Consequently, this allows for specific structural features to be targeted in the product by choosing an appropriate precursor.

The cation-exchange synthetic approach is thus broadly applicable to the incorporation of metal cations that have a strong tendency to disproportionate, oxidize in air, or to otherwise decompose in typical high temperature reactions needed to achieve sufficient ion diffusion. For example, this includes the synthesis of many new Sn(II)-containing oxides at low temperatures from cation exchange with halide salts [18, 19], such as reported for  $SnMO_3$  (M = Ti, Zr, Hf) perovskites [20,21]. Other examples include mixed-metal oxides containing Cu(I)-, Ag(I)-, and other cations that frequently are difficult to prepare at high temperatures [22,23]. Herein, the synthesis of a new Eu(II)-oxide is described that has been prepared through a flux-mediated cation exchange between a Na<sub>2</sub>Ta<sub>4</sub>O<sub>11</sub> precursor and EuBr<sub>2</sub>. To our knowledge, this represents the first reported investigation involving a cation-exchange reaction to synthesize a new divalent RE-containing oxide. Its structure has been determined by synchrotron powder X-ray diffraction to be generally isostructural with SrTa<sub>4</sub>O<sub>11</sub>. It is also found to contain Ta-vacancies that result in a partial oxidation of Eu(II) to Eu(III), as probed by temperature-dependent magnetic susceptibility, SEM-EDS and Mössbauer spectroscopy.

### 2. Experimental

### 2.1. Synthesis of Na<sub>2</sub>Ta<sub>4</sub>O<sub>11</sub>

 $Na_2Ta_4O_{11}$  was synthesized via a solid-state reaction using  $Na_2CO_3$  and  $Ta_2O_5$ . Stoichiometric amounts of the precursors were ground together using a mortar and pestle for  $\sim\!20$  min. The resulting mixture was placed into an alumina crucible and heated in a box furnace. The temperature was ramped to 1273 K over the course of 2 h and was subsequently held at 1273 K for 3 h. The furnace was then shut off and the products were allowed to radiatively cool to room temperature inside the furnace. The final product was again ground using a mortar and pestle prior to use in the next step.

# 2.2. Flux-mediated synthesis of $EuTa_{4-x}O_{11}$

The reactants, Na<sub>2</sub>Ta<sub>4</sub>O<sub>11</sub> and EuBr<sub>2</sub>, were ground together in an argon-filled glovebox in a 1:3 M ratio. The resulting powder mixture was then sealed into an evacuated fused silica ampoule under dynamic vacuum. The reactants were then ramped to 1173 K over a period of 1.5 h and held at this temperature for 24 h. The furnace was then turned off and the reaction vessel was allowed to radiatively cool to room temperature inside the furnace. The products were then washed and centrifuged several times with methanol to remove the NaBr side product and the remaining EuBr<sub>2</sub> flux. The remaining powder was dried under dynamic vacuum at room temperature. The powder was then reground inside the glovebox with additional EuBr<sub>2</sub> in a 1:3 ratio and the heating cycle was repeated. The powder was again washed with methanol and dried under vacuum to obtain the final product that was confirmed by powder XRD to have generally the same structure type as SrTa<sub>4</sub>O<sub>11</sub>, as described below. For comparison, solid state reactions using Eu, Eu<sub>2</sub>O<sub>3</sub> and Ta<sub>2</sub>O<sub>5</sub> yielded either no reaction and/or minor amounts of unidentified products when heated to temperatures from

1173 to 1273 K for 48 h.

### 2.3. Characterization

Laboratory powder X-ray diffraction data (PXRD) were collected on a Rigaku R-axis Spider diffractometer using Cu K $\alpha$  radiation ( $\lambda = 1.5418$ Å) from a sealed tube X-ray source (40 kV, 36 mA) and a curved imageplate detector. Synchrotron PXRD used for the Rietveld structural refinement was collected at the Advanced Photon Source at the 17-BM beamline with a wavelength of 0.241079 Å. Crystal structure refinements were performed using the Rietveld method in the GSAS-II software package [24]. The refinement proceeded by a fitting of the background function and sample displacement, followed by unit cell parameters, scale factor, atomic positions and isotropic displacement parameters. The Eu(II) cations were found to occupy two possible sites, Eu1 and Eu2 in Wyckoff sites 2d and 2b with respective percentages of 93.6(1)% and 6.4(1)%. These two Eu sites were constrained to have a total occupancy of unity. Further, refinement of the Ta crystallographic sites indicated that the Ta2 exhibited an occupancy of 95.8(1)%, or ~4.2% vacancies. These mixed-site and partial occupancies were found to be consistent with the mixed Eu(II)/Eu(III) oxidation states found in the magnetic susceptibility and Mössbauer spectroscopic data (see below). The final fitting converged to R and wR values of 4.70% and 8.22% with a phase fraction for EuTa<sub>4-x</sub>O<sub>11</sub> ( $x \sim 0.04$ ) of  $\sim 97.2\%$  and a ~2.8% impurity of EuTaO<sub>4</sub>. Full details of the final refinement results can be found in the Supporting Information.

UV–Vis diffuse reflectance measurements were taken on a Shimadzu UV-3600 spectrophotometer equipped with an integrating sphere. The background was a pressed barium sulfate disc. The data were transformed by using the Kubelka–Munk, F(R), function. Tauc plots of (F(R) x hv)<sup>n</sup> versus photon energy allow for the extraction of the direct (n=2) and indirect (n=1/2) bandgap transition energies to be determined. The direct and indirect transitions were determined by extrapolating the linear portion of the plot to the baseline. Elemental analysis was performed using a JOEL SM 6010LA scanning electron microscope which is equipped with a secondary electron imaging detector along with a JOEL silicon drift detector. The SEM EDS data were collected using a 20 kV accelerating voltage.

# 2.4. Magnetic susceptibility and Mössbauer spectroscopy

The magnetic susceptibilities of polycrystalline samples of nominally EuTa<sub>4-x</sub>O<sub>11</sub> were measured as a function of temperature and with external magnetic fields of 0.1, 1, 4 and 7 T with a MPMSX7 magnetometer (Quantum Design). The background of the sample holders was determined in separate runs and subtracted from the experimental data. A<sup>151</sup>Eu Mössbauer spectroscopic study on a sample, nominally EuTa<sub>4-x</sub>O<sub>11</sub>, was performed with a<sup>151</sup>Sm:EuF<sub>3</sub> source (21.53 keV transition, 55 MBq activity, 1% of the total activity). The measurement was performed in transmission geometry at 78 K using a liquid nitrogen-bath cryostat. The source was kept at room temperature. The sample was ground to a fine powder and mixed with  $\alpha$ -quartz to ensure an even distribution of the sample within the PMMA sample holder ( $\varnothing$  2 cm). The optimal sample thickness was calculated according to [25]. Fitting and plotting of the spectrum were done with the WinNormos for Igor6 program package [26] and graphical editing with CorelDRAW2017 [27].

### 2.5. Electronic structure calculations

Spin-polarized density functional theory calculations were performed by application of the projector augmented wave (PAW) method within the Vienna *Ab Initio* Simulation Package (VASP) [28,29]. Exchange correlation functionals were treated within the generalized gradient approximation (GGA) of Perdew, Burke and Ernzerhof [30]. To probe the energetics of the Eu-site occupation within the exchanged EuTa<sub>4</sub>O<sub>11</sub> crystal structure, calculations of the total energy were carried

out with the Eu cation located on either the 2d or the 2b Wyckoff sites, as well as a mixed-site model within a  $2\times2\times1$  superstructure. The 2d Wyckoff site is that reported for the Sr(II) cation within the SrTa<sub>4</sub>O<sub>11</sub> structure. The cutoff energy and criteria for energy convergence were set to 520 eV and  $10^{-8}$  eV, respectively. To represent the electron correlations of the Eu 4f states, an on-site repulsion parameter (DFT + Ueff method) of 6.0 eV was used. Full geometry relaxation calculations utilized a  $4\times4\times2$  k-point mesh, while densities-of-states (DOS) calculations were performed using an  $8\times8\times4$  k-point mesh. Band dispersion plots were constructed with 10 intersections along each of the high symmetry directions of the conventional k-point path ( $\Gamma$ -M-K- $\Gamma$ -A-L-H-A|L-M|H-K) in the Brillouin zone of the crystal system [31].

#### 3. Results and discussion

# 3.1. Synthesis and crystal structure

The synthesis of EuTa<sub>4</sub>O<sub>11</sub> from the Na<sub>2</sub>Ta<sub>4</sub>O<sub>11</sub> structure [32], which contains layers of TaO<sub>7</sub> pentagonal bipyramids, was investigated by flux-mediated cation exchange with EuBr2. The reaction can be represented by  $Na_2Ta_4O_{11}+EuBr_2 \rightarrow EuTa_4O_{11}+2$  NaBr. The exothermic formation of the stable NaBr side product provides a significant driving force for the reaction, with its removal easily achieved by washing in methanol to purify the product. This approach enabled a relatively low synthesis temperature of ~1173 K and time of 48 h, with the dark, brown-colored product exhibiting a powder XRD highly similar to that for SrTa<sub>4</sub>O<sub>11</sub>. While the syntheses of many Eu(II) oxides have been reportedly facilitated by reduction of Eu(III) precursors at much higher temperatures and reaction times, there is currently no reported Eu(III)-Ta-O phase with appropriate 1:4 stoichiometry of Eu:Ta that could potentially yield EuTa<sub>4</sub>O<sub>11</sub>. Thus, a flux-mediated cation exchange pathway is fundamental to the successful synthesis of EuTa<sub>4</sub>O<sub>11</sub>. Prior studies have demonstrated cation exchange reactions involving solids with the underlying structure type of  $\alpha$ -U<sub>3</sub>O<sub>8</sub>, e.g.,  $A_x$ Ta<sub>4</sub>O<sub>11</sub> and  $A_xTa_7O_{19}$  (x = 1, 2, 3; A = Cu(I), Ag(I), Pb(II), La(III)), and that the underlying tantalate substructure can be maintained [33,34]. However, the current study represents the first extension to a divalent RE cation.

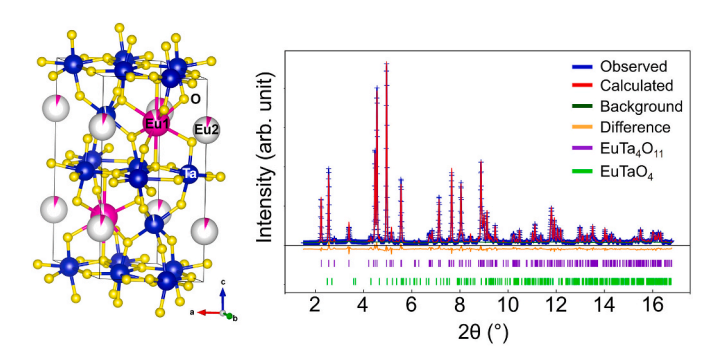


**Fig. 1.** Plot of Rietveld refinement of powder XRD data set (right) and crystal structure of  $EuTa_{4-x}O_{11}$  (left) with unit cell outlined and atom types labeled.

The final refined crystal structure of EuTa<sub>4-x</sub>O<sub>11</sub> (x = 0.042(1)) via Rietveld refinement of the synchrotron powder XRD data is shown in Fig. 1, alongside the fitted refinement plot. Listings of the lattice parameters, atom positions, and site occupancies are provided in Table 1. The cation-exchanged EuTa<sub>4-x</sub>O<sub>11</sub> structure was initially modeled to have the known structure type of SrTa<sub>4</sub>O<sub>11</sub> in the space group P6<sub>3</sub>22 (#182). Many Eu(II) and Sr(II) oxides are isostructural owing to their nearly identical ionic radii of 125 pm and 126 pm, respectively, for eight-fold coordination. The SEM EDS data, Fig. S1/Table S1, reveals no detectable Na signal, with a chemical composition that is in qualitative agreement. However, results of Rietveld refinements suggest two partially occupied crystallographic sites for the Eu(II) cations, Eu1 and Eu2. The first site, Eu1, is the primary site with 0.936(1) occupancy, while the alternate Eu2 site shows a 0.064(1) occupancy. The occupation of a secondary A-site between the TaO<sub>7</sub> pentagonal layers is unique for EuTa<sub>4-x</sub>O<sub>11</sub>, as this feature has not been observed in the Sr(II) analog. By comparison, these sites are both fully occupied by Na cations in the parent Na<sub>2</sub>Ta<sub>4</sub>O<sub>11</sub> structure and suggesting the Eu(II)-cation sites are thus impacted by the starting structure. The Eu1 and Eu2 sites also have different coordination environments, as shown in Fig. 2. The primary site, Eu1, has an 8-fold coordination with six shorter Eu – O distances of 2.49(2) Å and two longer Eu – O distances of 2.65(4) Å. Conversely, the Eu2 site has six symmetry-equivalent Eu - O distances of 2.84(3) Å, resulting in a flattened octahedral EuO6 coordination and O - Eu - O angles of 103.2° around the 3-fold axis. Based on structural analyses of prior Eu(II) oxides, the Eu(II) cation most commonly prefers coordination numbers higher than six, which provides more space for Eu(II). The preferential site occupation of the Eu cation in EuTa<sub>4-x</sub>O<sub>11</sub> for the Eu1 sites with 8-fold coordination is consistent with this observation. Refinement results also indicate a small Ta deficiency on the Ta2 site, with a refined occupation of 0.958(1). The refined composition is thus EuTa<sub>4-x</sub>O<sub>11</sub> (x = 0.042(1); ~1% Ta vacancies) or Eu<sub>0.8</sub><sup>III</sup>Eu<sub>0.2</sub>Ta<sub>3.96(1)</sub>O<sub>11</sub>, with ~20% oxidation of Eu(II) to Eu(III) from charge balance considerations. Prior studies have also shown similar non-stoichiometries with Eu(II)/Eu(III) mixtures in niobate and tantalate products obtained from solid state reactions [35].

Density-functional theory calculations were employed to better understand the underlying energetic differences in the preferential Eu occupation over the two different crystallographic sites. The modeled structure with 100% occupancy of the Eu1 site (-323.855 eV f.u. $^{-1}$ ) is substantially lower in energy than the model with occupancy of the Eu2 site (-322.561 f.u. $^{-1}$ ), by -1.294 eV Eu $^{-1}$ . Thus, there is a clear energetic preference for the Eu(II) cation to be located at the Eu1 site over the Eu2 site. A third model, where the Eu was randomly distributed across both Eu sites was also modeled, leads to an energy (-322.658 eV f.u. $^{-1}$ ) slightly lower than the Eu2 model but still significantly higher in energy than the Eu1 model. The results are thus consistent with preferential occupancy of the Eu1 site.

This leads to the question, why is the Eu2 site at higher energy even partially occupied? The occupation of the Eu2 site can likely be attributed to the structure of the  $Na_2Ta_4O_{11}$  precursor. The structure of  $Na_2Ta_4O_{11}$  is nearly identical to that of  $EuTa_{4-x}O_{11}$ . The primary difference is that unlike  $EuTa_{4-x}O_{11}$ , in which only a single Eu-site is occupied, both A-sites are fully occupied in  $Na_2Ta_4O_{11}$ . This is

**Table 1** Listing of refined atomic coordinates, site occupancies and isotropic displacement parameters ( $\mathring{A}^2$ ) for EuTa<sub>4-x</sub>O<sub>11</sub> (x=0.042(1)) with lattice parameters a=6.2539(2)  $\mathring{A}$  and c=12.3417(2)  $\mathring{A}$  in space group  $P6_322$ .

Atom	x	у	z	Occupancy	Site Mult.	$U_{iso}$
Eu1	1/3	2/3	3/4	0.936(1)	2d	0.0095(1)
Eu2	0	0	3/4	0.064(1)	2b	0.0095(1)
Ta1	0	0.3574(5)	0	1.0	6g	0.0064(2)
Ta2	1/3	2/3	1/4	0.958(1)	2c	0.0064(2)
01	0.055(3)	0.435(5)	0.1524(9)	1.0	12 <i>i</i>	0.018(3)
O2	0	0.263(5)	1/2	1.0	6g	0.018(3)
O3	1/3	2/3	0.535(3)	1.0	4 <i>f</i>	0.018(3)

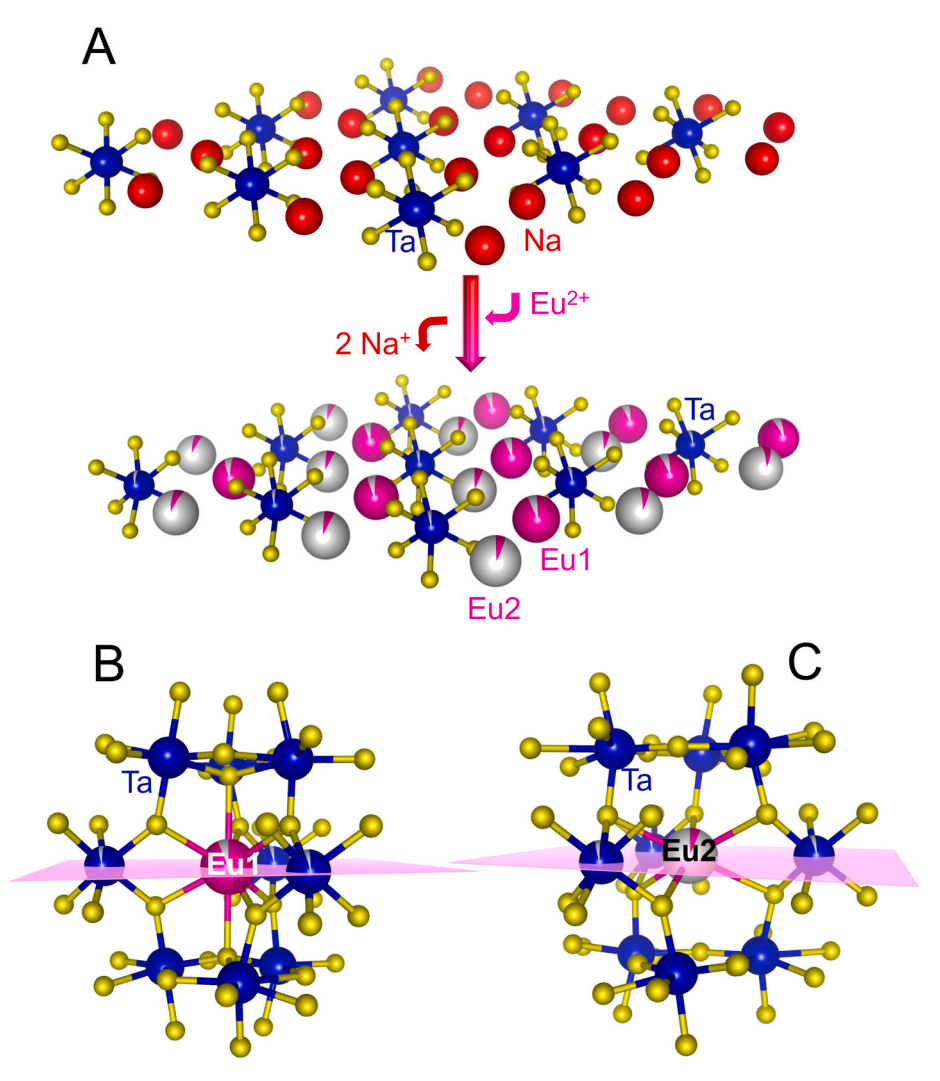
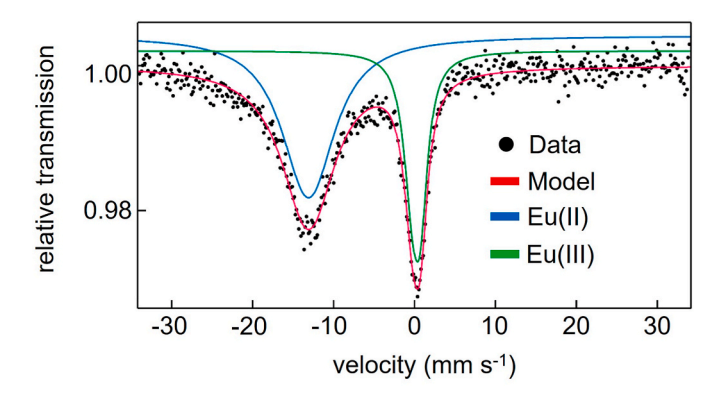


Fig. 2. Structural views of the layers of  $TaO_6$  octahedra and Na or Eu cations in  $Na_2Ta_4O_{11}$  and  $EuTa_{4.x}O_{11}$  (A), and the local coordination geometries of Eu1 (B; 93.6% occupied) and Eu2 (C; 6.4% occupied).

illustrated in Fig. 2A, which shows the Na/TaO<sub>6</sub> layer of the Na<sub>2</sub>Ta<sub>4</sub>O<sub>11</sub> structure (the full structure of Na<sub>2</sub>Ta<sub>4</sub>O<sub>11</sub> can be seen in Fig. S1). This exchange reaction does not involve isovalent cations, so a single Eu(II) cation replaces two Na(I) cations in the structure. Cation mobility within these layers has been previously reported [36], and here is shown to coincide with the Ta vacancies on the intralayer octahedral sites. The Eu (II) cation can then either occupy the Na1(Eu1) or Na2(Eu2) site. As described above, there is a strong energy preference for the Eu1 site. However, these calculations were performed at 0 K and only consider the electronic energy of a static structure. When additional factors such as elevated temperature or changes in local chemical composition during the exchange are considered, it is likely that some small fraction of Eu(II) cations can exchange onto the Na2/Eu2 site. These Eu(II) cations are then kinetically trapped as the sample is cooled to ambient temperature. Consequently, the presence of the secondary Eu2 site can likely be attributed to the mechanisms of the ion-exchange reaction and the structure of the Na<sub>2</sub>Ta<sub>4</sub>O<sub>11</sub> precursor.

### 3.2. Mössbauer spectroscopy and magnetic susceptibility

Characterization of the EuTa<sub>4-x</sub>O<sub>11</sub> powder by  $^{151}$ Eu Mössbauer spectroscopy and magnetic susceptibility measurements were used to further probe the oxidation state of the Eu cations. The  $^{151}$ Eu Mössbauer spectrum of the EuTa<sub>4-x</sub>O<sub>11</sub> sample at 78 K is presented in Fig. 3 along with a transmission integral fit. The corresponding fitting parameters



**Fig. 3.** Experimental (dots) and simulated (red)  $^{151}$ Eu Mössbauer spectrum of EuTa<sub>4-x</sub>O<sub>11</sub> at 78 K. Green line is a fitting of Eu(III), the blue line of Eu(II) and the entire model in red.

are summarized in Table 2. The spectrum shows two well separated contributions, fitted as the blue and green lines. The sub-signal at  $\delta=0.23(2)~{\rm mm~s^{-1}}$  (green) is in a typical range of Eu(III) compounds [37]. The signal is subjected to quadrupole splitting of  $\Delta E_{\rm Q}=2.5(2)~{\rm mm~s^{-1}}$  (a consequence of the low site symmetry 3.2 on Wyckoff site 2c) and its experimental line width of  $\Gamma=2.2(1)~{\rm mm~s^{-1}}$  is in the usual range. The

**Table 2** Fitting parameters of  $^{151}$ Eu Mössbauer spectroscopic measurements at 78 K of the EuTa<sub>4-x</sub>O<sub>11</sub> sample.  $\delta=$  isomer shift,  $\Delta E_{\rm Q}=$  electric quadrupole splitting,  $\Gamma=$  experimental line width.

Signal	δ/mm·s <sup>-1</sup>	$\Delta E_Q/mm \cdot s^{-1}$	Γ/mm·s <sup>-1</sup>	Area/%
Blue	-13.11(5)	2.5 <sup>a</sup>	7.6(2)	69(1)
Green	0.23(2)	2.5(2)	2.2(1)	31(1)

 $<sup>^{\</sup>rm a}~\Delta E_{\rm Q}$  of the Eu(II) sub-signal was constrained to the same value as for the Eu (III) sub-signal.

sub-signal located at  $\delta=-13.11(5)~{\rm mm~s}^{-1}$  is due to Eu(II) [37], similar to the one measured for EuMoO<sub>4</sub> ( $-13.98(16)~{\rm mm~s}^{-1}$ ), Eu<sub>2</sub>SiO<sub>4</sub> ( $-13.47(9)~{\rm mm~s}^{-1}$ ) [38] or Eu<sub>2</sub>LnTaO<sub>6</sub> ( $-12.3~{\rm mm~s}^{-1}$ ) [10]. The Eu(II): Eu(III) ratio is 69(1): 31(1) and again, this situation is comparable to Eu<sub>3</sub>TaO<sub>6</sub> and its isotypic niobium compound [10]. When accounting for the ~5% impurity of EuTaO<sub>4</sub>, then ~26% of the Eu(III) signal arises from EuTa<sub>4-x</sub>O<sub>11</sub>. The percentage of Eu(III) for EuTa<sub>4-x</sub>O<sub>11</sub> yields an x=0.06, or ~1.5% Ta vacancies, in reasonable agreement with the Rietveld refinement results.

The striking feature in this <sup>151</sup>Eu Mössbauer spectrum is the line width of the Eu(II) sub-signal. It is well known that the quadrupole splitting parameter and the line width correlate. To obtain a stable fit, the quadrupole splitting parameter of the Eu(II) sub-signal was constrained to the same value as for Eu(III), resulting in a line width value of  $\Gamma = 7.6(2) \text{ mm s}^{-1}$ . A simple refinement with solely a distribution of isomer shifts (and constrained small line width) can be ruled out, since such a fit would yield physically unreasonably low isomer shifts. The broad Eu(II) signal is thus the envelope, which accounts for the manifold of cations in different electronic environments. Such a large line broadening has also been observed for Eu-containing fluorozirconate glasses [39]. Similar to these glasses, the line broadening for the EuTa<sub>4-x</sub>O<sub>11</sub> sample most likely is an interplay of different parameters: (i) an isomer shift distribution in a small range due to changes in the EuO8 coordination sphere (slightly varying  $\mathrm{Eu^{II}}$ -O distances) as a consequence of small defects of the tantalum sites (Fig. 2B), (ii) unresolved quadrupole splitting, and (iii) possible charge fluctuations between divalent and trivalent europium.

Temperature dependent magnetic susceptibility measurements were used to further probe the mixed-valent Eu(II)/Eu(III) oxidation states and the potential for magnetic frustration. Given that the Eu cations form a triangular arrangement, there is the potential for magnetic frustration in EuTa<sub>4-x</sub>O<sub>11</sub>. Recent work on the structurally related NdTa<sub>7</sub>O<sub>19</sub>, which also crystallizes with an  $\alpha$ -U<sub>3</sub>O<sub>8</sub> structure, has been shown to display magnetic frustration of the Nd(III) cations that results in spin liquid behavior [40]. Plotted in Fig. 4 is the inverse molar magnetic susceptibility of EuTa<sub>4-x</sub>O<sub>11</sub> versus the temperature, which follows a paramagnetic behavior that can be fitted by the Curie-Weiss

expression, where *C* is the Curie constant given by:

$$C = \frac{N_{\rm A} \mu_0 \mu_{\rm B}^2 \, \mu_{\rm eff}^2}{3k_{\rm B}},$$
 eq. (1)

with  $N_A$  being Avogadro's constant,  $\mu_0$  the permeability of the vacuum,  $\mu_B$  the Bohr magneton,  $k_B$  the Boltzmann constant, and  $\mu_{\rm eff}$  the effective magnetic moment. The data showed a slight field dependence (see Fig. 4 (left) which we attribute to minute traces of a ferromagnetic impurity. These were corrected for using a Honda-Owen extrapolation ( $\mu_0 H \to \infty$ ) [41,42]. The initial fitting of the magnetic susceptibilities in the temperature interval of 100–300 K gave a Curie-Weiss temperature of -10 K, suggesting weak predominant antiferromagnetic exchange between the magnetic centers. The obtained magnetic moment ( $\mu_{\rm eff}$ ) of 6.2  $\mu_B$  per Eu atom is smaller than the theoretical moment of Eu(II) which is 7.94  $\mu_B$ . We ascribe this deviation to the presence of Eu(III) cations, which have a smaller effective magnetic moment, which is also temperature dependent. Details are provided in the Supporting Information. The susceptibility data were modeled assuming a mixture of Eu(II) and Eu(III) oxidation states, according to:

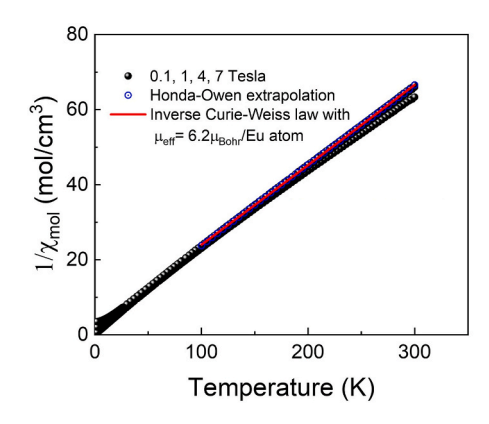
$$\chi_{\text{mol}}(T) = (1 - x_{\text{III}}) \chi_{\text{mol,III}}(T) + x_{\text{III}} \chi_{\text{mol,III}}(T) + \chi_0,$$
 eq. (2)

where  $\chi_0$  represents the imagnetic contribution from the electrons in the closed shells and  $x_{\rm III}$  gives the fraction of Eu(III) cations.  $\chi_{\rm mol,II}(T)$  and  $\chi_{\rm mol,III}(T)$  are given in the SI. Using Pascal's increments for the ions in their respective oxidation state [43] we obtain a  $\chi_0$  value of -210  $\times$  10<sup>-6</sup> cm<sup>3</sup>/mol. Fitting the Honda-Owen corrected molar magnetic susceptibility data to Eq. (1) results in a value for  $\chi_{\rm III}$  of about 50%, see Fig. 4 (right), with a good fit over the whole temperature range.

Slight deviations from the Curie-Weiss law becoming apparent below  ${\sim}100\,$  K and are accounted for by Eq. (1) owing to the temperature dependent effective moment of Eu(III). This concentration of Eu(III) could be explained by  ${\sim}2.5\%$  Ta vacancies in EuTa<sub>4-x</sub>O<sub>11</sub>, while also not entirely accounting for the contribution of Eu(III) in the few percent EuTaO<sub>4</sub> impurity. These data agree reasonably well with other experimental data for EuTa<sub>4-x</sub>O<sub>11</sub> when considering the typical variability between samples, and the very large impact of the Ta vacancy concentration on the Eu(II) to Eu(III) ratio.

### 3.3. Optical bandgap and electronic structure

UV–visible diffuse reflectance measurements were taken to determine the underlying changes in the band gap from  $Na_2Ta_4O_{11}$  (white color) to  $EuTa_{4-x}O_{11}$  (brown/black color) resulting from the cation exchange reaction with  $EuBr_2$ . The recorded absorption data set was transformed using the Kubelka-Munk function (F(R)). These transformed data were used to generate Tauc plots to obtain either the direct (n=2) or indirect (n=1/2) transition energies, and which indicated



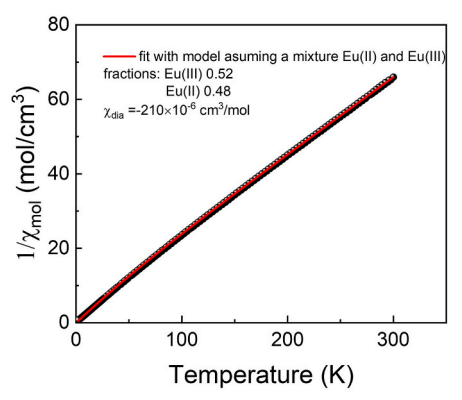
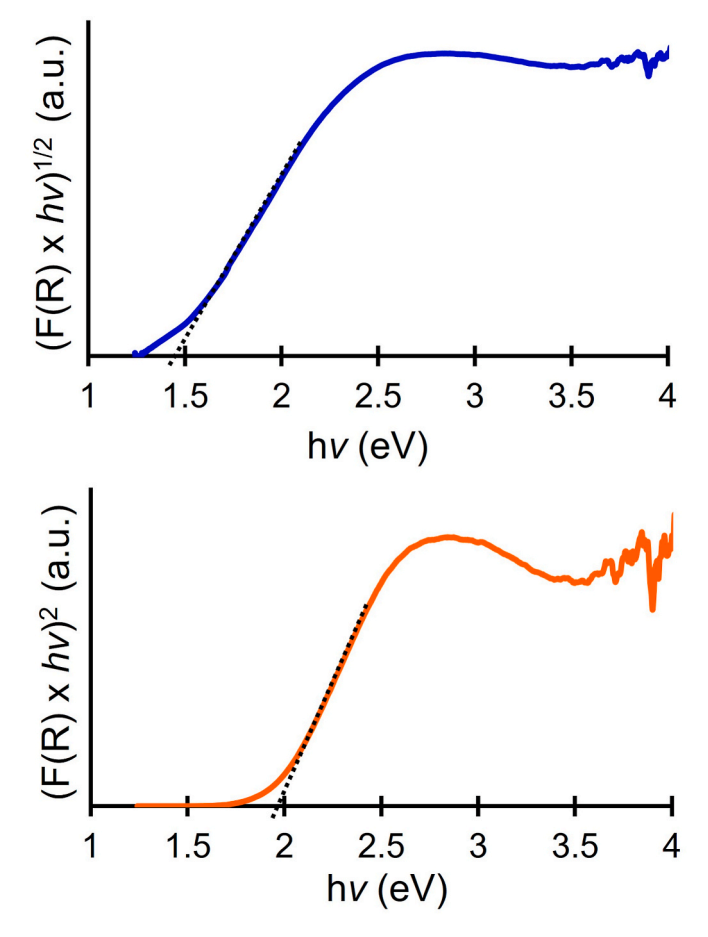


Fig. 4. Inverse magnetic susceptibility of EuTa<sub>4-x</sub>O<sub>11</sub> (black circles) as a function of temperature measured at magnetic fields of 0.1, 1, 4 and 7 T. Red lines represent fittings using the inverse Cure-Weiss law (left) and as a mixture of Eu(II)/Eu(III) (right).



**Fig. 5.** Optical diffuse reflectance data for  $EuTa_{4,x}O_{11}$  shown as Tauc plots of the indirect (upper) and direct (lower) bandgap transitions.

consistency with semiconducting-type optical behavior. The transition energies in each plot can be determined by extrapolating the linear portion of the data to the baseline. These fits are marked by dashed lines in the Tauc plots shown in Fig. 5. The indirect transition in  $EuTa_{4-x}O_{11}$  was found to be  $\sim\!1.46$  eV, while the direct transition is at a higher energy of  $\sim\!1.93$  eV. The dark brown color of the  $EuTa_{4-x}O_{11}$  powder is consistent with this measured small band gap and thus revealed a surprisingly large  $\sim\!2.6$  eV redshift compared to  $Na_2Ta_4O_{11}$  with a UV bandgap of  $\sim\!4.1$  eV.

Spin-polarized DFT calculations of the electronic structure for EuTa $_4$ <sub>x</sub>O $_{11}$  were used to obtain a deeper understanding of the origin of its large redshift in band gap. As described above, idealized structural models were constructed from the refined crystal structure, with the Eu cation located on either the Eu1 site (lowest energy), Eu2 site (highest energy), or a mixture of both (intermediate energy). The resulting band structure and densities-of-states plots for the energetically-preferred Eu1

structural model are shown together in Fig. 6. The electronic structure reveals a Eu-based, spin polarized (i.e., up spin), valence band (VB) that is localized over the half-filled  $4f^7$  orbitals. This is consistent with a Eu (II) oxidation state. Conversely, the conduction band (CB) edge is delocalized over primarily the empty Ta-based 5d orbitals mixed, with increasing O 2p contributions at higher energies. The underestimation of semiconductor bandgaps using DFT methods is well established [44]. The energetic gap spanning these VB and CB states is significantly underestimated at  $\sim$ 0.289 eV (indirect; ( $\Gamma \rightarrow$  H–K(midpoint)), principally stemming from electronic transitions between the Eu  $4f^7$  to Ta  $5d^0$  states, respectively. The direct bandgap transition occurs at a slightly higher energy of 0.325 eV. These trends are consistent with the optical direct and indirect transitions in Fig. 5.

By comparison, the electronic structure profiles of the alternative structural models containing Eu2 or mixed-Eu1/Eu2 site occupancies are very similar to that described above for the Eu1-site model. Each shows the same atomic contributions to the CB and VB states in their DOS plots (spin polarized), as given in the Supporting Information. However, these structural models exhibit relatively higher energies of their VB states by  $\sim 0.15$  eV. This originates from a decrease in the coordination of the Eu cation from 8-fold to 6-fold, Fig. 2(B and C), and leading to an increased energy for the O 2p orbitals. As a result, the delocalization of the CB edge over the Ta 5d states were closely similar, but also increased by  $\sim$ 0.2 eV in energy by comparison. The reported electronic structure of Na<sub>2</sub>Ta<sub>4</sub>O<sub>11</sub> [32] shows an analogous Ta-based CB, but its VB is delocalized entirely over the O 2p orbitals. The introduction of higher-energy Eu  $4f^7$  orbitals as a new VB, i.e., by the reaction with EuBr<sub>2</sub>, has thus yielded the significant redshift of the band gap and an energetically preferred occupation of the Eu1 site with the higher coordination number. However, it should be noted that all structural models were calculated to be thermodynamically stable with respect to decomposition to the binary oxides.

### 4. Conclusions

A cation-exchange route to a new Eu(II)-containing oxide, EuTa<sub>4</sub>. <sub>x</sub>O<sub>11</sub>, has been investigated as an alternative to more traditional highertemperature reactions involving EuO and highly reducing atmospheres. Rather, its synthesis can be achieved by the topotactic reaction of a precursor oxide, Na<sub>2</sub>Ta<sub>4</sub>O<sub>11</sub>, with the Eu(II)-containing halide salt EuBr<sub>2</sub>. Rietveld refinements show the exchange of one Eu(II) for two Na cations and a preferential occupation of the Na1/Eu1 site (~94%) as compared to the Na2/Eu2 site (~6%). Also, a small concentration (~1-2%) of Ta-vacancies forms within the layers of Eu cations and isolated TaO<sub>6</sub> octahedra, with these layers constituting the likely cationexchange pathway. As a result, a partial oxidation of Eu(II) to Eu(III) is found by Mössbauer spectroscopy and temperature-dependent magnetic susceptibility measurements. The exchange reaction also results in a large redshift of the bandgap to  $\sim$ 1.46 eV with the introduction of the 4f orbitals of Eu as a higher-energy valence band. In summary, these results demonstrate a synthetic pathway that can help unlock the door to many new Eu(II)-containing oxides with potentially interesting magnetic and optical properties.

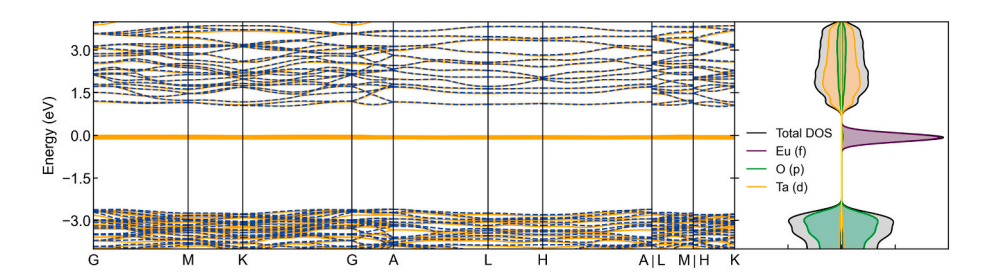


Fig. 6. Calculated spin-polarized band structure diagram with up-spin (yellow) and down-spin (blue) bands and densities-of-states (DOS; right) diagram with individual atomic orbital contributions projected out for Eu (purple), O (green), Ta (yellow) and the net DOS in black. The Fermi level is set at 0 eV.

#### CRediT authorship contribution statement

Shaun O'Donnell: Investigation, Writing – review & editing. Eric Gabilondo: Investigation, Writing – review & editing. Subhendu Jana: Investigation, Writing – review & editing. Aylin Koldemir: Writing – review & editing. Theresa Block: Writing – review & editing. Myung-Hwan Whangbo: Methodology, Writing – review & editing. Reinhard Kremer: Writing – review & editing. Rainer Pöttgen: Writing – review & editing. Paul A. Maggard: Investiation, Writing – review & editing.

#### Declaration of competing interest

The authors declare that they have no known competing financial interests or personal relationships that could have appeared to influence the work reported in this paper.

### Data availability

Data will be made available on request.

# Acknowledgments

The authors acknowledge primary support of this work from the National Science Foundation (DMR-2317605). This research used resources of the Advanced Photon Source, a U.S. Department of Energy (DOE) Office of Science user facility operated for the DOE Office of Science by Argonne National Laboratory under Contract No. DE-AC02-06CH11357. The authors would also like to thank Andriy Zakutayev (NREL) and Chris Rom (NREL) for access to the APS and Wenqian Xu for assistance at APS during the experiment. Additional components of this research were performed in part at the Analytical Instrumentation Facility (AIF) at North Carolina State University, which is supported by the State of North Carolina and the National Science Foundation (Award ECCS-2025064). The AIF is a member of the North Carolina Research Triangle Nanotechnology Network (RTNN), a site in the National Nanotechnology Coordinated Infrastructure (NNCI).

# Appendix A. Supplementary data

Supplementary data to this article can be found online at https://doi.org/10.1016/j.jssc.2023.124338.

### References

- [1] J.S. Gardner, M.J.P. Gingras, J.E. Greedan, Magnetic pyrochlore oxides, Rev. Mod. Phys. 82 (2010) 53–107.
- [2] C.N.R. Rao, A.K. Cheetham, R. Mahesh, Giant magnetoresistance and related properties of rare-earth manganates and other oxide systems, Chem. Mater. 8 (1996) 2421–2432.
- [3] M.W. Shafer, Preparation and crystal chemistry of divalent europium compounds, J. Appl. Phys. 36 (1965) 1145–1152.
- [4] J.E. Greedan, J. McCarthy, C. Sipe, Complex oxides containing divalent europium. II. Eu(M,M')O<sub>3</sub> phases, Inorg. Chem. 14 (1975) 775–779.
- [5] T.R. McGuire, B.E. Argyle, M.W. Shafer, J.S. Smart, Magnetic properties of some divalent europium compounds, J. Appl. Phys. 34 (1963) 1345–1346.
- [6] B.T. Matthias, R.M. Bozorth, Ferromagnetic interaction in EuO, Phys. Rev. Lett. 7 (1961) 160–161.
- [7] M.W. Shafer, T.R. Mcguire, J.C. Suits, Europium orthosilicate, A new transparent ferromagnet, Phys. Rev. Lett. 11 (1963) 251–252.
- [8] T. Katsufuji, H. Takagi, Coupling between magnetism and dielectric properties in quantum paraelectric EuTiO<sub>3</sub>, Phys. Rev. B 64 (2001), 054415.
- [9] P.G. Reuvekamp, R.K. Kremer, J. Köhler, A. Bussmann-Holder, Spin-lattice coupling induced crossover from negative to positive magnetostriction in EuTiO<sub>3</sub>, Phys. Rev. B 90 (2014), 094420.
- [10] Y. Misawa, Y. Doi, Y. Hinatsu, Magnetic ordering of divalent europium in double perovskite Eu<sub>2</sub>LnTaO<sub>6</sub> (Ln=Rare earths) magnetic interactions of Eu<sup>2+</sup> ions determined by magnetic susceptibility, specific heat, and <sup>151</sup>Eu mössbauer spectrum measurements, J. Solid State Chem. 184 (2011) 1478–1483.
- [11] T. Kolodiazhnyi, H. Sakurai, Y. Matsushita, Structure, magnetism, specific heat, and dielectric properties of Eu<sub>2</sub>Ta<sub>2</sub>O<sub>7</sub>, Appl. Phys. Lett. 105 (2014), 202903.

- [12] G.J. McCarthy, J.E. Greedan, Complex oxides containing divalent europium. I. Guideline for the prediction of new phases. Application to phases of the type  $EuMO_3$ , Inorg. Chem. 14 (1975) 772–775.
- [13] W.A. England, J.B. Goodenough, P.J. Wiseman, Ion-exchange reactions of mixed oxides, J. Solid State Chem. 49 (1983) 289–299.
- [14] J. Gopalakrishnan, Chemie douce approaches to the synthesis of metastable oxide materials, Chem. Mater. 7 (1995) 1265–1275.
- [15] P.A. Maggard, Capturing metastable oxide semiconductors for applications in solar energy conversion, Acc. Chem. Res. 54 (2021) 3160–3171.
- [16] E. Gabilondo, S. O'Donnell, R. Newell, R. Broughton, M. Mateus, J.L. Jones, P. A. Maggard, Renaissance of topotactic ion-exchange for functional solids with close packed structures, Chem. Eur J. 28 (1–6) (2022), e202200479.
- [17] J.R. Chamorro, T.M. McQueen, Progress toward solid state synthesis by design, Acc. Chem. Res. 51 (2018) 2918–2925.
- [18] Y. Zou, J. Le, Y. Cao, N. An, Y. Zhou, J. Li, D. Liu, Y. Kuang, Tetragonal tungsten bronze type Sn(II)-Based quaternary oxides: a new class of visibile-light-absorbing semiconductors for photoelectrochemical water oxidation, J. Mater. Chem. A 9 (2021) 21085–21093.
- [19] S. Uma, J. Singh, V. Thakrai, Facile room temperature ion-exchange synthesis of Sn<sup>2+</sup> incorporated pyrochlore-type oxides and their photocatalytic activities, Inorg. Chem. 48 (2009) 11624–11630.
- [20] S.C. O'Donnell, C.-C. Chung, A. Carbone, R. Broughton, J.L. Jones, P.A. Maggard, Pushing the limits of metastability in semiconducting perovskite oxides for visiblelight-driven water oxidation, Chem. Mater. 32 (2020) 3054–3064.
- [21] E.A. Gabilondo, S. O'Donnell, R. Broughton, J.L. Jones, P.A. Maggard, Synthesis and stability of Sn(II)-Containing perovskites: (Ba,Sn<sup>II</sup>)HfO<sub>3</sub> versus (Ba,Sn<sup>II</sup>)SnO<sub>3</sub>, J. Solid State Chem. 302 (1–10) (2021), 122419.
- [22] S. O'Donnell, R.K. Kremer, P.A. Maggard, Metastability and photoelectrochemical properties of Cu<sub>2</sub>SnO<sub>3</sub> and Cu<sub>2.x</sub>Li<sub>x</sub>TiO<sub>3</sub>. Two Cu(I)-Based oxides with delafossite structures, Chem. Mater. 35 (2023) 1404–1416.
- [23] D. Arney, P.A. Maggard, Effect of platelet-shaped surfaces and silver-cation exchange on the photocatalytic hydrogen production of RbLaNb<sub>2</sub>O<sub>7</sub>, ACS Catal. 2 (2012) 1711–1717.
- [24] B.H. Toby, R.B. Von Dreele, GSAS-II: the genesis of a modern open-source all purpose crystallography software package, J. Appl. Crystallogr. 46 (2013) 544–549.
- [25] G.J. Long, T.E. Cranshaw, G. Longworth, Mössbauer Eff. Ref. Data J. 6 (1983)
- [26] R.A. Brand, WinNormos for Igor6 (Version for Igor6.2 or above: 22.02.2017), Universität Duisburg, Duisburg, Germany, 2017.
- [27] CORELDRAW Graphics Suite 2017 (Version 19.0.0.328), Corel Corporation, Ottawa, Ontario (Canada), 2017.
- [28] G. Kresse, J. Furthmüller, Efficient iterative schemes for Ab Initio total-energy calculations using a plane-wave basis set, Phys. Rev. B Condens. Matter 54 (1996) 11169–11186.
- [29] G. Kresse, J. Furthmüller, Efficiency of ab-initio total energy calculations for metals and semiconductors using a plane-wave basis set, Comput. Mater. Sci. 6 (1996) 15–50.
- [30] J.P. Perdew, K. Burke, M. Ernzerhof, Generalized gradient approximation made simple, Phys. Rev. Lett. 77 (1996) 3865–3868.
- [31] Y. Hinuma, G. Pizzi, Y. Kumagai, F. Oba, I. Tanaka, Band structure diagrams paths based on crystallography, Comput. Mater. Sci. 128 (2017) 140–184.
- [32] N. McLamb, P.P. Sahoo, L. Fuoco, P.A. Maggard, Flux growth of single-crystal Na<sub>2</sub>Ta<sub>4</sub>O<sub>11</sub> particles and their photocatalytic hydrogen production, Cryst. Growth Des. 13 (2013) 2322–2326.
- [33] W. Stemmer, R. Gruehn, Exchange reactions of ternary tantalates and niobates with halide melts – a way to new lead tantalates, Z. Anorg. Allg. Chem. 619 (1993) 409–415
- [34] J. Boltersdorf, P.A. Maggard, Structural and electronic investigations of PbTa<sub>4</sub>O<sub>11</sub> and BiTa<sub>7</sub>O<sub>19</sub> constructed from α-U<sub>3</sub>O<sub>8</sub> types of layers, J. Solid State Chem. 229 (2015) 310–321.
- [35] N.N. Greenwood, F. Viegas, F. Studer, The oxidation state of europium in niobates and tantalates having the tetragonal tungsten-bronze structure, J. Solid State Chem. 31 (1980) 347–353.
- [36] I. Sullivan, P.P. Sahoo, L. Fuoco, A.S. Hewitt, S. Stuart, D. Dougherty, P. A. Maggard, Cu-deficiency in the p-type semiconductor Cu<sub>5-x</sub>Ta<sub>11</sub>O<sub>30</sub>; impact on its crystalline structure, surfaces, and photoelectrochemical properties, Chem. Mater. 26 (2014) 6711–6721.
- [37] N.N. Greenwood, T.C. Gibb, Mössbauer Spectroscopy, Chapman and Hall, London,
- [38] G. Gerth, P. Kienle, K. Luchner, Chemical effects on the isomer shift in <sup>151</sup>Eu, Phys. Lett. 27 (1968) 557–558.
- [39] J.M.D. Coey, A. McEvoy, M.W. Shafer, Mössbauer study of europium in fluorozirconate glass, J. Non-Cryst. Solids 43 (1981) 387–392.
- [40] T. Arh, B. Sana, M. Pregelj, P. Khuntia, Z. Jaglicic, P.K. Biswas, P. Manuel, L. Mangin-Thro, A. Ozarowski, A. Zorko, The Ising triangular-lattice antiferromagnet neodymium heptatantalate as a quantum spin liquid candidate, Nat. Mater. 21 (2022) 416–422.
- [41] M. Owen, Magnetochemische untersuchungen. Die thermomagnetischen eigenschaften der elemente, Ann. Phys. 37 (1912) 657–699.
- [42] K. Honda, Susceptibility of the elements, Ann. Phys. 32 (1910) 1027-1063.
- [43] G.A. Bain, J.F. Berry, Diamagnetic corrections and Pascal's constants, J. Chem. Educ. 85 (2008) 532–536.
- [44] J.P. Perdew, Density functional theory and the band gap problem, Int. J. Quant. Chem. 28 (1985) 497–523.